



HAL
open science

Osteoclast-Derived Autotaxin, a Distinguishing Factor for Inflammatory Bone Loss

Sacha Flammier, Olivier Peyruchaud, Fanny Bourguillault, François Duboeuf,
Jean-Luc Davignon, Derek Norman, Sylvie Isaac, Hubert Marotte, Gabor
Tigyi, Irma Machuca-gayet, et al.

► **To cite this version:**

Sacha Flammier, Olivier Peyruchaud, Fanny Bourguillault, François Duboeuf, Jean-Luc Davignon, et al.. Osteoclast-Derived Autotaxin, a Distinguishing Factor for Inflammatory Bone Loss. *Arthritis & rheumatology*, 2019, 71 (11), pp.1801-1811. 10.1002/art.41005 . hal-02354473

HAL Id: hal-02354473

<https://hal.science/hal-02354473>

Submitted on 12 Feb 2020

HAL is a multi-disciplinary open access archive for the deposit and dissemination of scientific research documents, whether they are published or not. The documents may come from teaching and research institutions in France or abroad, or from public or private research centers.

L'archive ouverte pluridisciplinaire **HAL**, est destinée au dépôt et à la diffusion de documents scientifiques de niveau recherche, publiés ou non, émanant des établissements d'enseignement et de recherche français ou étrangers, des laboratoires publics ou privés.

Osteoclast-derived Autotaxin, a distinguishing factor for inflammatory bone loss

Sacha FLAMMIER^{1,2¶}, PhD, Olivier PEYRUCHAUD^{1,2¶}, PhD, Fanny BOURGUILLAULT^{1,2}, MS, François DUBOEUF^{1,2}, PhD, Jean-Luc DAVIGNON^{3,4,5}, MD, PhD, Derek D NORMAN⁶, PhD, Sylvie ISAAC⁷, MD, Hubert MAROTTE^{8,9,10}, MD, PhD, Gabor TIGYI⁶, PhD, Irma MACHUCA-GAYET^{1,2§*}, PhD, Fabienne COURY^{1,2,11§*}, MD, PhD.

¹INSERM UMR1033 LYOS, Lyon, France

²University of Lyon I, Lyon, France

³University of Paul Sabatier Toulouse III, Toulouse, France

⁴INSERM - CNRS U1043, CPTP, CHU Purpan, Toulouse, France

⁵Department of Rheumatology, Pierre Paul Riquet Hospital, Toulouse, France

⁶Department of Physiology, University of Tennessee Health Sciences Center, Memphis, Tennessee, USA

⁷Department of Anatomical Pathology, Lyon Sud Hospital, Pierre-Bénite, France

⁸SAINBIOSE, INSERM, U1059, LBTO, Saint-Etienne, France

⁹University of Lyon, Saint-Etienne, France

¹⁰Department of Rheumatology, University Hospital of Saint-Etienne, Saint-Etienne, France

¹¹Department of Rheumatology, Lyon Sud Hospital, Pierre-Bénite, France

¶Contributed equally to this work

§Contributed equally to this work

* Corresponding authors:

Fabienne COURY

Email: fabienne.coury-lucas@chu-lyon.fr; fabienne.coury@free.fr

ORCID : 0000-0002-9175-8620

And

Irma MACHUCA-GAYET

Email: irma.machuca-gayet@inserm.fr

ORCID : 0000-0002-3010-9774

INSERM UMR1033

UFR de Médecine Lyon Est

Rue Guillaume Paradin

69372 Lyon Cedex 08, France

Phone: +33 (0)4 78 77 86 72

Fax: +33 (0)4 78 77 86 63

ABSTRACT

Objective The severity of rheumatoid arthritis (RA) correlates directly with bone erosions due to osteoclast (OC) hyperactivity. Despite controlled inflammation, RA patients in sustained clinical remission or low disease activity may continue to accrue erosions urging the need for treatments suitable for long-lasting inhibition of OC activity without altering their physiological function in bone remodeling. Autotaxin (ATX) contributes to inflammation but its role in bone erosion is unknown.

Methods ATX was targeted by both treatments with pharmacological drugs and conditional inactivation of *Ennp2* (ATX gene) in OC (Δ ATX^{Ctsk} mice). Arthritic and erosive diseases were studied in human tumor necrosis factor transgenic (*hTNF*^{+/-}) and K/BxN serum-transfer arthritis mice. Systemic bone loss was also analyzed in the Lipopolysaccharide (LPS)-induced inflammation and estrogen deprivation models. Joint inflammation and bone erosion were assessed by histology and microcomputed tomography. The role of ATX was examined in murine OC differentiation and activity assays.

Results OC present at inflammatory sites overexpressed ATX. Pharmacological inhibition of ATX significantly mitigated focal (36% amelioration; $p < 0.05$) and systemic bone loss (43% amelioration; $p < 0.05$) in *hTNF*^{+/-} mice without affecting synovial inflammation. OC-derived ATX revealed instrumental in OC bone resorptive activity and was upregulated under inflammation elicited by TNF or LPS. Specific loss of ATX in OC significantly protected against systemic bone loss and erosion after LPS and K/BxN-treatment (30% in systemic bone loss; $p < 0.01$ and 55% in erosion; $p < 0,001$) without bone protective property following ovariectomy.

Conclusions Our results identify ATX as a novel OC factor that specifically controls inflammation-induced bone erosions and systemic bone loss. Therefore, ATX inhibition offers a novel therapeutic approach for preventing bone erosion in RA.

Keywords: *autotaxin, osteoclast, bone loss, rheumatoid arthritis.*

INTRODUCTION

Rheumatoid arthritis (RA) is a chronic relapsing disease characterized by synovial inflammation, focal bone degradation, and systemic osteoporosis. Irreversible periarticular bone erosion is a hallmark of RA, which can occur soon after disease onset and correlates with disease severity and functional deterioration. At the present time, treatments of RA are focused on the inhibition of inflammation to halt synovitis and subsequent progression of bone erosion. However, some patients in sustained clinical remission still develop radiographic erosions (1, 2).

Osteoclasts (OC) are responsible for focal erosions, juxtaarticular bone loss, and systemic osteoporosis in RA (3-5). Significant evidence has accumulated demonstrating that OC are present at sites of focal bone erosion at the pannus-bone interface (3, 6-8). These multinucleated cells originate from fusion of myeloid cells under the control of receptor activator of nuclear factor- κ B ligand (RANKL) and proinflammatory cytokines in RA (5). Current treatments of RA are largely limited to controlling the inhibition of the immune inflammation to halt synovitis and to delay or even stop subsequent progression of bone erosion. Denosumab, a neutralizing antibody that selectively binds RANKL and consequently inhibits OC formation, slows the progression of bone erosion in RA patients without affecting synovial inflammation, suggesting that it is possible to limit bone erosion by targeting OC (9, 10). However current anti-resorptive drugs are suboptimal in RA as they could lead to atypical fractures due to shutting down physiologic bone remodeling pointing to the need for alternative therapies.

Autotaxin (ATX), also known as ecto-nucleotide pyrophosphatase/phosphodiesterase-2 (ENPP2), is a secreted enzyme produced by various tissues including the brain, liver, and adipose tissue (11). ATX is also a lysophospholipase D responsible for cleavage of lysophosphatidylcholine (LPC) to lysophosphatidic acid (LPA) that in turn acts as a growth factor with pleiotropic actions such as cell proliferation, differentiation, and migration via at least six G protein-coupled receptors (LPA₁₋₆) (12-13). High levels of LPA and ATX have been detected in synovial fluids of RA patients (14-16) and LPA₁ knock out mice were reported to be protected from collagen-induced arthritis (14) suggesting that LPA/ATX axis controls inflammatory arthritis pathogenesis. ATX is upregulated by TNF in synovial fibroblasts resulting in increased levels of ATX at the joint inflammatory site in mouse models of RA (16). Thus, the contribution of ATX to synovial inflammation has been well established. In contrast, its role in bone erosion occurrence is not yet resolved. In case of an action, it could be either secondary to TNF dependent inflammation or direct on osteoclast-mediated bone resorption. Actually, LPA is a serum borne factor mandatory *in vitro* for RANKL-induced OC formation (17). Also, LPA mediates

OC survival (18) and controls OC resorption activity through cytoskeleton organization (19, 20). However, the origin of LPA in bone is still unknown.

In the present study we show that OC produces functionally active ATX. Using both genetic and pharmacological approaches we find that blocking ATX prevents systemic bone loss and bone erosion under inflammatory conditions accompanying RA without interfering with physiologic non-inflammatory bone remodeling. We provide evidence that OC-derived ATX is a key regulator whose inhibition uncouples inflammation from bone resorption. Therefore, ATX is a promising therapeutic target for the prevention of inflammation-associated bone loss and of bone erosion in RA.

MATERIALS AND METHODS

Mice

Enpp2^{fl/fl} mice were kindly provided by Dr. Moolenaar (NKI, Amsterdam, Netherlands) (21). The *Enpp2^{fl}* allele was deleted specifically in OC by crossing the strain with mice that express the Cre recombinase under the control of the Cathepsin K promoter, kindly provided by Dr. Kato (Tokyo University, Japan) (22). Spontaneous arthritic *Tg197* humanized TNF transgenic (*hTNF^{+/-}*) mice were obtained from Dr Kollias (A. F. B. S. Center, Athens, Greece) (23). *Enpp2^{fl/fl}* and *Ctsk-Cre^{+/-}* mouse strains were maintained on a BalB/c genetic background while *hTNF^{+/-}* mouse strain was on the C57/BL6 background. Four-month-old female *CTRL* (*Enpp2^{fl/fl}Ctsk-Cre^{-/-}*) and Δ *ATX^{Ctsk}* (*Enpp2^{fl/fl}Ctsk-Cre^{+/-}*) mice underwent ovariectomy (OVX) or sham-OVX surgery and were euthanized after 1 month. Uterine weight was measured at necropsy. Animals were sacrificed following the ARRIVE guidelines. Experimental protocols were approved by the local ethical Committee, CECCAPP of the Ecole Normale Supérieure or by the Institutional Animal Care and Use Committee of the Université Claude Bernard Lyon-1 (Lyon, France).

Animal models of inflammation and arthritis

Six-week-old male *CTRL* and Δ *ATX^{Ctsk}* mice were injected i.p. either with 5mg/kg lipopolysaccharide (LPS, Sigma-Aldrich) or with a phosphate buffered saline (PBS) vehicle on day 0 and day 4 and euthanized on day 8.

Both inducible and spontaneous animal models of arthritis were used in this study. K/BxN serum-transfer arthritis model was induced in 7-week-old male mice as previously described (24) by i.p. injection of 7 μ l/g of pooled K/BxN arthritogenic serum on days 0, 2, 7, 12. Mice were euthanized on day 17 after initial injection. Twenty three day-old *hTNF^{+/-}* female mice (23) were i.p. daily treated with either the ATX inhibitor BMP22 (1 mg/kg/day) or PBS vehicle for 14 days and euthanized on day 14 after the first injection. Disease severity and weight

loss in both arthritis models was blindly monitored every 2 to 3 days by a single investigator (SF). Clinical score was assessed by using the following system: 0, normal; 1, mild redness or swelling of digits, midfoot or ankle; 2, moderate inflammation of digits, midfoot or ankle; 3, moderate to severe inflammation involving digits; 4, severe inflammation of entire paw resulting in ankylosis. Each hind limb was graded, giving a maximum possible score of 8 per animal. Micrometer caliper was used to measure ankle thickness (25).

Microquantitative computed tomography (micro-CT)

Micro-CT analyses of the talus or calcaneus and of the distal femur of arthritic mice were carried out using a micro-CT scanner Skyscan 1176 (Skyscan Inc.). The X-ray excitation voltage was set to 50 kV with a current of 500 mA. A 0.5 mm aluminum filter was used to reduce beam-hardening artifacts. Samples were scanned in 70% ethanol with a voxel size of 9.08 μm . Section images were reconstructed with NRecon software (version 1.6.1.8, Skyscan). Three-dimensional modeling and analysis of bone volume to tissue volume or bone volume density (BV / TV), and bone surface to tissue volume or bone surface density (BS / TV) were obtained with the CTAn (version 1.9) and CTVol (version 2.0) softwares. TV was determined as the volume in the absence of erosions and bone surface density was used to measure surface roughness/erosion as described in Quan et al. (26).

Histologic analysis

Mouse joint tissue and bone samples were fixed, decalcified, and embedded in paraffin. Cytochemical detection of TRAP positive OC using the TRAP activity kit assay (Sigma-Aldrich) and immunohistochemical detection of ATX using polyclonal anti-ATX antibody (Cayman) were performed. The resorption surface (Oc.S/BS) was calculated as the ratio of TRAP-positive trabecular bone surface (Oc.S) to the total trabecular BS using image J software. Inflammation and bone erosions were assessed on HPS-stained sagittal sections of the midfoot in a blinded fashion from two independent reviewers (OP, FC) using a semiquantitative scoring system as previously described (7), with scores of 0-5 for inflammation and of 0–5 for bone resorption.

Osteoclastogenesis and bone resorption assays

Murine osteoclastogenesis and resorption assays were carried out as described previously (20, 27). Briefly, BMMC from hind limbs of mice were collected and seeded in 96-well tissue culture plates at a density of 2×10^4 cells per well in α -MEM medium (Invitrogen). We used charcoal-stripped FBS to avoid LPA and LPC contaminations of the cell culture medium. Culture media were supplemented with or without LPC (1 μM , Avanti Polar Lipids) recombinant ATX (rATX, 0.3nM), Ki16425 (10 μM , Interchim), or PF8380 (10nM, Cayman

Chemicals). After 6 days, mature OC were enumerated under a microscope on the basis of the number of nuclei (≥ 3 nuclei) and the TRAP activity (Sigma-Aldrich). Results were expressed as the number of OC per well. For stimulation experiments, OC were stimulated for 6h with recombinant mouse TNF (R&D systems) or LPS (Sigma-Aldrich) after one hour serum starvation in presence or absence of TCPA-1 (2 μ M) (Sigma-Aldrich). All osteoclastogenesis experiments were performed in triplicate.

For resorption experiments, resorbed surface was quantified on bone-mimicking Osteo Assay Surface (3988; Corning). Day-4 OC were detached from plastic wells by flushing after incubation at 37°C for 5 min in PBS plus 0.25 mM EDTA, counted, and then seeded at the same number (2×10^4 cells/well in 96-well plates) in replicate plates and cultured for 48h. To measure the total surface of the resorbed matrix, OC were washed off with distilled water, and then the matrix was stained with a 5% (wt/vol) silver nitrate solution. Finally, the resorption index was obtained by expressing the total resorbed area per well. Images of all substrates were numerized with Epsilon perfection V750 Pro scanner (Micro Epsilon, Ortenburg, Germany), and manually quantified with ImageJ (National Institutes of Health, Bethesda, MD, USA).

Western blotting

The protein concentration of cell extracts was determined with a Protein Assay kit (Biorad). Cellular extracts from cultured OC were separated by 8% SDS-PAGE and transferred to immobilon transfer membrane (Millipore). Membranes were incubated with 5% low fat-milk and 0.1% Triton X-100, pH 7.4 in PBS for one hour at room temperature followed by an overnight incubation with anti-ATX antibody (Cayman chemicals) or with anti- β actin antibody (Sigma-Aldrich). ATX and β actin were visualized using horseradish-peroxidase-donkey anti-rabbit IgG or anti-mouse IgG (Jackson) and enhanced chemiluminescence (Amersham).

Real-time quantitative polymerase chain reaction (RT-qPCR) analysis.

Total RNA from OC cultures and from powdered whole bone was extracted using Trizol (Invitrogen AB) and the Nucleospin RNAII kit (Macherey-Nagel). Complementary DNA from OC and bones were synthesized by reverse transcription using iScript cDNA Synthesis kit (Biorad). Expression of target genes was quantified by qRT-PCR on a Biorad CFX Connect Real Time system using the iTaq Universal SYBR Green Super Mix (Biorad) and sets of specific primers. Quantifications were normalized to corresponding RNA L32 values and expressed as relative expression using the $2^{-\Delta\Delta C(T)}$ method (27). Primer sequences (designated as f, forward, and as r, reverse) were as follows: L32 (f, 5'-CAAGGAGCTGGAGGTGCTGC-3' ; r, 5'-CTGCTCTTTCTACAATGGC-3'), *Enpp2* (f, 5'-GCCCTGATGTCCGTGTATCT-3'; r, 5'-CGTTTGAAGGCAGGGTACAT-3'), *Ctsk* (f, 5'-

GAGGGCCAACTCAAGAAGAA-3' ; r, 5'- GCCGTGGCGTTATACATACA-3'), *Acp5* (f, 5'- CAGCAGCCCAAATGCCT-3' ; r, 5'- TTTTGAGCCAGGACAGCTGA-3').

Statistical analysis

Differences between groups were determined by 1-way or 2-way ANOVA followed by Bonferroni posttest using GraphPad Prism v5.0c software. Single comparisons were carried out using two-sided unpaired Mann Whitney Test. $P < 0.05$ was considered significant.

RESULTS

Pharmacological inhibition of ATX activity reduces TNF-induced focal erosion and systemic bone loss without interfering with synovitis

TNF plays an important role in the initiation and progression of inflammation and destructive bone loss in RA. To evaluate the therapeutic utility of inhibiting ATX in inflammatory arthritis, we blocked ATX activity using a small molecule inhibitor BMP22 in an inflammatory model of arthritis driven by TNF overexpression, the *hTNF*^{+/-} transgenic mice (23). The therapeutic potential of blocking ATX activity with BMP22 has been previously demonstrated in non-inflammatory mouse models (28, 29). We observed that treatment with 1mg/kg/day BMP22 for 14 days of *hTNF*^{+/-} transgenic mice did not substantially affect inflammation, as monitored by weight loss, paw swelling, clinical arthritis score, and hind paw histopathology compared with controls (Fig. 1A and 1B). Nevertheless, the histopathologic bone erosion score was significantly reduced in BMP22-treated mice (Fig. 1B bottom right panel). In support of these observations, micro-CT analysis and bone surface to bone tissue volume ratio (BS/TV) quantification in the calcaneum revealed that BMP22 was significantly protective (36% decrease; $p < 0.05$) against the cortical bone erosion of *hTNF*^{+/-} mice (Fig. 1C). Furthermore, BMP22 treatment significantly decreased TNF-induced systemic bone loss with a significant increase of 43% in BV/TV in BMP22-treated mice compared with vehicle-treated animals ($p < 0.05$) (Fig. 1D). Consistently, the number of tartrate resistant acid phosphatase (TRAP)-positive multinucleated OC was significantly reduced in the long bones of *hTNF*^{+/-} mice treated with BMP22 compared to vehicle-treated animals (Fig. 1E). To determine the origin of ATX in the osteoarticular environment, we analyzed serial histological sections from *hTNF*^{+/-} transgenic mice and found high ATX expression at the site of synovial inflammation (Fig. 1F left panel). Strikingly, at the bone erosion sites in the vicinity of synovial inflammation, TRAP-positive multinucleated OC displayed strong ATX expression (Fig. 1F right panel).

OC-derived ATX is functionally active in resorbing OC.

ATX was found to be a late marker of OC differentiation as shown by increased expression of the *Enpp2* gene and ATX protein during osteoclastogenesis reaching the highest level on day 5 in mature OC *in vitro* (Fig. 2A and inset). ATX generates LPA leading to activation of LPA receptors (30). We have previously demonstrated that LPA is a serum-borne factor required *in vitro* for RANKL-mediated osteoclastogenesis and osteoclastic bone resorption via activation of the LPA₁ receptor (17, 20). Therefore, we investigated whether ATX expressed by OC could affect OC differentiation and bone resorption. LPA and LPA precursors such as LPC are abundant in serum, therefore all OC manipulations were performed in the presence of charcoal-treated serum in order to eliminate the lipid fraction. In these conditions, osteoclastogenesis and mineral matrix resorption were abrogated (Fig. 2B-C). In this system using wild type bone marrow mononuclear cells (BMMC), no increase of OC number was observed when LPC the substrate of ATX was added to the culture medium indicating that OC-derived ATX failed to affect osteoclastogenesis directly (Fig. 2B). This can potentially be explained by the low levels of ATX expression at early stages of OC differentiation (Fig. 2A). Nevertheless, the combination of LPC with exogenous recombinant ATX (rATX) restored almost 80% of the osteoclastogenesis observed with non-delipidated serum. The effect of LPC+rATX was completely abolished in the presence either of the ATX inhibitor PF-8380 or the LPA_{1/3} antagonist Ki16425 (Fig. 2B). These results indicate that ATX present in OC environment generates functionally active LPA which in turn regulates osteoclastogenesis. With regard to bone resorptive activity, mature OC were generated first in the presence of normal serum and then re-plated on synthetic mineralized surfaces in the presence of charcoal-stripped serum. Under these conditions, LPC alone was remarkably potent in restoring 80% of the lost resorptive activity of wild type OC generated in charcoal-treated serum (Fig. 2C). A 20% additional enhancement was observed in the presence of LPC supplemented with rATX, suggesting that endogenously ATX produced by OC was the most effective. PF-8380 and Ki16425 treatments abolished the effects of exogenous LPC or LPC plus rATX, and rATX by itself had no effect. These data indicate that OC-derived ATX is not required during the initial steps of osteoclastogenesis but generates functionally active LPA that promotes bone resorption by mature OC by acting via the LPA₁ receptor.

Selective inhibition of OC-derived ATX does not affect physiological bone mass and ovariectomy-induced bone loss.

To further elucidate the role of ATX in OC, we generated mice lacking ATX in mature OC by the crossing of *Enpp2^{fl/fl}* mice with *Ctsk-Cre^{+/-}* mice. These conditional KO *Enpp2^{fl/fl} Ctsk-Cre^{+/-}* mice (referred hereafter as Δ ATX^{Ctsk} mice) were born at the expected birth rate (not shown) which is different from the germline-deficient *Enpp2* mice that display lethality during

embryogenesis due to severe vascular and neuronal defects (21, 31). ATX expression was assessed *in vitro* during the differentiation of BMMC into OC showing an almost complete absence of the protein in mature OC (Fig. 3A). Consistent with the previous results on bone resorption from wild type OC in the presence of the ATX inhibitor (Fig. 2C), ATX-deficient OC were unable to resorb mineralized matrix in the presence of LPC alone whereas, addition of rATX rescued this phenotype (Fig. 3B). Surprisingly, quantitative computed microtomography (micro-CT) measurements of bone density and quantification of OC numbers in control (*CTRL*) and Δ ATX^{Ctsk} animals did not reveal any differences (Fig. 3C). Remarkably, sham and ovariectomized *CTRL* and Δ ATX^{Ctsk} mice did not show any differences in bone volume density measured by micro-CT (Fig. 3D). Thus, selective deletion of OC-derived ATX has no impact on bone mass under non-pathologic physiological and ovariectomy-induced osteoporotic conditions.

Selective inhibition of OC-derived ATX prevents LPS-induced bone loss

Because pharmacological inhibition of ATX activity protected *hTNF*^{+/-} mice from bone erosion and systemic bone loss (Fig. 1), we hypothesized that potential regulation of bone mass by ATX might only manifest under inflammatory conditions. We first generated and harvested *CTRL* and Δ ATX^{Ctsk} mature OC that were secondary plated on mineralized matrix in the presence of LPC and charcoal-stripped serum supplemented with or without TNF or LPS. Compared with *CTRL* OC whose bone resorptive activity was significantly enhanced by TNF and LPS, ATX-deficient OC were refractory to stimulation either by TNF or LPS (Fig. 4A). To extend this finding in the context of inflammation-dependent OC resorption *in vivo*, we treated *CTRL* and Δ ATX^{Ctsk} mice to endotoxin LPS challenge (5mg/kg). As expected, LPS induced a drastic bone loss with 40% reduction in BV/TV in *CTRL* mice compared with vehicle-treated mice (32). In contrast, LPS-treated Δ ATX^{Ctsk} mice displayed no significant trabecular bone mass reduction similar to vehicle-treated animals (Fig. 4B). LPS-treated *CTRL* mice exhibited a significant increase in OC surface per bone surface (OC.S/BS) compared to mice treated with the vehicle, whereas Δ ATX^{Ctsk} mice challenged with LPS showed no change in OC content compared to vehicle-treated Δ ATX^{Ctsk} mice (Fig. 4C). LPS treatment induced a significant increase in expression of late osteoclastic markers, *Acp5* and *CtsK*, and of *Enpp2* in the bone from *CTRL* mice, but not from Δ ATX^{Ctsk} mice (Fig. 4D). Remarkably, we observed a significant increase of *Enpp2* transcript induced by LPS only in *CTRL* mice, indicating that among the bone cells expressing *Enpp2*, the OC is most responsive to LPS challenge. To evaluate whether the inflammatory environment affected *Enpp2* expression in OC, mature *CTRL* OC were treated either with TNF or LPS in the presence of LPC and charcoal-treated serum. Both treatments upregulated *Enpp2* in mature

OC indicating that *Enpp2* promoter was the target of TNF and LPS signalling pathways in these fully differentiated cells (Fig. 4E). This hypothesis was confirmed by the use of TCPA-1, a selective inhibitor of I κ B kinase (IKK) β , which completely abolished both TNF- and LPS-induced *Enpp2* expression (Fig. 4E).

Selective deletion of OC-derived ATX impacts bone mass and erosion under arthritic inflammation

Next, we investigated if OC-derived ATX could contribute to arthritis-induced bone loss. *CTRL* and Δ ATX^{*Ctsk*} mice given serum from K/BxN mice were then used to induce an arthritic disease (24). In line with the results obtained in the LPS model, under these extreme inflammatory conditions, micro-CT analysis showed that K/BxN serum transfer elicited a severe 88% decrease in BV/TV trabecular bone mass in *CTRL* mice. In contrast, serum transfer was significantly less detrimental causing a 58% decrease in BV/TV in Δ ATX^{*Ctsk*} animals indicating a significant protection of 30% ($p < 0,01$) in Δ ATX^{*Ctsk*} from systemic bone loss induced by K/BxN serum (Fig. 5A). Δ ATX^{*Ctsk*} mice treated with K/BxN serum displayed similar paw swelling, clinical arthritis score and histological synovitis compared to control mice underscoring that OC-derived ATX does not impact the inflammatory process (Fig. 5B-C top panel). Remarkably, Δ ATX^{*Ctsk*} mice displayed less TRAP-positive multinucleated OC at the synovitis-bone interface than *CTRL* mice and significant protection against cortical erosion induced by K/BxN serum (Fig. 5C bottom panel-D). Talus BS/TV values from *CTRL* mice treated with K/BxN serum showed a significant 1.8-fold increase compared to vehicle-treated controls. Elevation of BS/TV ratio was due to increase in bone surface dependent on roughness/bone cortical erosions. Remarkably, increase in talus BS/TV value in Δ ATX^{*Ctsk*} mice induced by K/BxN serum transfer was significantly reduced by 55% compared to that observed in *CTRL* mice ($p < 0.001$) (Fig. 5E). Altogether these results indicate that OC-derived ATX did not contribute to the inflammatory process but controlled arthritic bone destruction, highlighting the possibility of ATX as a novel therapeutic target for the control of RA-associated bone loss.

DISCUSSION

The hypothesis for a major contribution of LPA and ATX in RA has emerged recently (14, 16). Mice with global deletion of the *Lpar1* gene do not develop arthritis following immunization with type II collagen due to mitigated immune cell infiltration (14). By using these LPA₁-deficient mice and pharmacological LPA₁ blocking drugs, we have previously shown that this receptor is a key effector of OC-mediated bone resorption (20). In addition,

TNF-driven ATX expression in synovial fibroblasts generates LPA that in turn activates synovial fibroblasts (14, 16). Thus, combined LPA and TNF signaling might contribute to joint inflammation and potentially to joint destruction. Indeed, genetic and pharmacological targeting of LPA₁ result in attenuated bone degradation in animal models of arthritis (14).

Data from preclinical animal arthritis models challenged with ATX inhibitor compounds have been lacking so far. Our study represents an important advance over the conditional genetic ablation of ATX in mesenchymal cells model described previously (16). The hypothesis put forward in that report, would predict attenuation of the inflammation after ATX inhibitor treatment. However, here we found that treatment with the inhibitor, BMP22 did not significantly affect articular inflammation in *hTNF^{+/-}* mice. This could have been due to a suboptimal dosing regiment. However, BMP22-treated *hTNF^{+/-}* mice displayed a significant reduction of local bone erosion and of systemic bone loss. Thus, pharmacological inhibition of ATX with BMP22 protected *hTNF^{+/-}* transgenic mice from inflammation-induced bone loss by mitigating osteoclastic bone resorption rather than affecting the inflammatory response. Therefore, inhibition of ATX using BMP22 caused distinctively different effects on inflammation versus bone resorption in this model of RA.

Bone erosions constitute a key and irreversible outcome in RA and reflect on the tight interaction between immune system and bone remodeling. Controlling synovial inflammation can arrest the progression of bone erosions in RA. However, RA patients in sustained clinical remission or low disease activity often continue to accrue bone erosions. In addition, certain RA patients exhibit persistent chronic synovitis marked by joint swelling without complaint of joint tenderness (33). Therefore, it might be worthwhile to consider the development of alternative therapeutics that selectively and directly target bone erosion. Indeed, current anti-resorptive drugs, such as bisphosphonates and denosumab, can lead to atypical fracture due to shutting down physiologic bone remodeling after long-term treatment.

No induction of toxicity was observed during this work with BMP22 nor reported from experimental mouse models of cancers using blockers of ATX activity (28, 34, 35). Furthermore, GLPG1690, a first-in-class ATX inhibitor, has successfully completed phase II clinical evaluation for the treatment of idiopathic pulmonary fibrosis without noted side effects (36). Therefore, pharmacological blocking of ATX activity is likely to also be safe in RA patients.

ATX was found to be a late osteoclastic marker explaining the absence of its impact on the differentiation of Δ ATX^{Ctsk} OC. In contrast, Δ ATX^{Ctsk} mature OC were remarkably defective in mineral matrix degradation that was potently rescued when supplied with exogenous ATX. Additional sources of ATX and/or LPA might also be available in the bone microenvironment originating from chondrocytes (37), osteoblasts (38), adipocytes (39) and

endothelial cells (40), that may partly explain the absence of bone phenotype of ΔATX^{Ctsk} mice. Surprisingly, specific inhibition of OC-derived ATX, did not protect ΔATX^{Ctsk} mice from osteoporosis induced by ovariectomy whereas in striking contrast to full protection of the animals in models of LPS- and K/BxN serum transfer-induced bone loss. This suggests that OC-derived ATX might be central to a remarkable specificity of inflammation over estrogen-dependent regulation of OC activity and bone degradation. Indeed, TNF and LPS enhanced the resorption activity by 6 to 7 fold in *CTRL* OC but were ineffective in ΔATX^{Ctsk} OC. This contention was supported by the presence of NF- κ B DNA binding sites on *Enpp2* promoter sequence (41) and was confirmed experimentally by the use of TCPA-1, a selective inhibitor of I κ B kinase (IKK) β , which totally blunted LPS- and TNF-enhanced ATX expression indicating a convergent regulation mechanism for *Enpp2* expression by both LPS and TNF in mature OC.

Collectively our results demonstrate that osteoclast-derived ATX is a key player in inflammatory osteoclast-mediated bone resorption and should be considered as a promising novel therapeutic target for halting bone erosion in RA.

REFERENCES

1. Cohen G, Gossec L, Dougados M, Cantagrel A, Goupille P, Daures JP, et al. Radiological damage in patients with rheumatoid arthritis on sustained remission. *Ann Rheum Dis* 2007;66:358–3.
2. Molenaar ET, Voskuyl AE, Dinant HJ, Bezemer PD, Boers M, Dijkmans BA. Progression of radiologic damage in patients with rheumatoid arthritis in clinical remission. *Arthritis Rheum* 2004;50:36–42.
3. Gravallese EM, Harada Y, Wang JT, Gorn AH, Thornhill TS, Goldring SR. Identification of cell types responsible for bone resorption in rheumatoid arthritis and juvenile rheumatoid arthritis. *Am J Pathol* 1998;152:943–51.
4. Goldring SR, Gravallese EM. Bisphosphonates: environmental protection for the joint? *Arthritis Rheum* 2004;50:2044–47.
5. Schett G, Hayer S, Zwerina J, Redlich K, Smolen JS. Mechanisms of Disease: the link between RANKL and arthritic bone disease. *Nat Clin Pract Rheumatol* 2005;1:47–54.
6. Bromley M, Woolley DE. Chondroclasts and osteoclasts at subchondral sites of erosion in the rheumatoid joint. *Arthritis Rheum* 1984;27:968–75.
7. Pettit AR, Ji H, von Stechow D, Müller R, Goldring SR, Choi Y, et al. TRANCE/RANKL knockout mice are protected from bone erosion in a serum transfer model of arthritis. *Am J Pathol* 2001;159:1689–99.
8. Redlich K, Hayer S, Maier A, Dunstan CR, Tohidast-Akrad M, Lang S, et al. Tumor necrosis factor alpha-mediated joint destruction is inhibited by targeting osteoclasts with osteoprotegerin. *Arthritis Rheum* 2002;46:785–92.

9. Deodhar A, Dore RK, Mandel D, Schechtman J, Shergy W, Trapp R, et al. Denosumab-mediated increase in hand bone mineral density associated with decreased progression of bone erosion in rheumatoid arthritis patients. *Arthritis Care Res* 2010;62:569–74.
10. Cohen SB, Dore RK, Lane NE, Ory PA, Peterfy CG, Sharp JT, et al. Denosumab Rheumatoid Arthritis Study Group. Denosumab treatment effects on structural damage, bone mineral density, and bone turnover in rheumatoid arthritis: a twelve-month, multicenter, randomized, double-blind, placebo-controlled, phase II clinical trial. *Arthritis Rheum* 2008;58:1299–309.
11. Giganti A, Rodriguez M, Fould B, Moulharat N, Cogé F, Chomarat P, et al. Murine and human autotaxin alpha, beta, and gamma isoforms: gene organization, tissue distribution, and biochemical characterization. *J Biol Chem* 2008;283:7776–89.
12. Umezu-Goto M, Kishi Y, Taira A, Hama K, Dohmae N, Takio K, et al. Autotaxin has lysophospholipase D activity leading to tumor cell growth and motility by lysophosphatidic acid production. *J Cell Biol* 2002;158:227–33.
13. Moolenaar WH, Hla T. SnapShot: Bioactive lysophospholipids. *Cell* 2012;148:378.e2.
14. Miyabe Y, Miyabe C, Iwai Y, Takayasu A, Fukuda S, Yokoyama W, et al. Necessity of lysophosphatidic acid receptor 1 for development of arthritis. *Arthritis Rheum* 2013;65:2037–47.
15. Zhao C, Fernandes MJ, Prestwich GD, Turgeon M, Di Battista J, Clair T, et al. Regulation of lysophosphatidic acid receptor expression and function in human synoviocytes: implications for rheumatoid arthritis? *Mol Pharmacol* 2008;73:587–600.
16. Nikitopoulou I, Oikonomou N, Karouzakis E, Sevastou I, Nikolaidou-Katsaridou N, Zhao Z, et al. Autotaxin expression from synovial fibroblasts is essential for the pathogenesis of modeled arthritis. *J Exp Med* 2012;209:925–33.
17. David M, Wannecq E, Descotes F, Jansen S, Deux B, Ribeiro J, et al. Cancer cell expression of autotaxin controls bone metastasis formation in mouse through lysophosphatidic acid-dependent activation of osteoclasts. *PloS One* 2010;5:e9741.
18. Lapierre DM, Tanabe N, Pereverzev A, Spencer M, Shugg RP, Dixon SJ, et al. Lysophosphatidic acid signals through multiple receptors in osteoclasts to elevate cytosolic calcium concentration, evoke retraction, and promote cell survival. *J Biol Chem* 2010;285:25792–801.
19. McMichael BK, Meyer SM, Lee BS. c-Src-mediated phosphorylation of thyroid hormone receptor-interacting protein 6 (TRIP6) promotes osteoclast sealing zone formation. *J Biol Chem* 2010;285:26641–51.
20. David M, Machuca-Gayet I, Kikuta J, Ottewell P, Mima F, Leblanc R, et al. Lysophosphatidic acid receptor type 1 (LPA1) plays a functional role in osteoclast differentiation and bone resorption activity. *J Biol Chem* 2014;289:6551–64.
21. van Meeteren LA, Ruurs P, Stortelers C, Bouwman P, van Rooijen MA, Pradère JP, et al. Autotaxin, a secreted lysophospholipase D, is essential for blood vessel formation during development. *Mol Cell Biol* 2006;26:5015–22.

22. Nakamura T, Imai Y, Matsumoto T, Sato S, Takeuchi K, Igarashi K, et al. Estrogen prevents bone loss via estrogen receptor alpha and induction of Fas ligand in osteoclasts. *Cell* 2007;130:811–23.
23. Keffer J, Probert L, Cazlaris H, Georgopoulos S, Kaslaris E, Kioussis D, et al. Transgenic mice expressing human tumour necrosis factor: a predictive genetic model of arthritis. *EMBO J* 1991;10:4025–31.
24. Monach PA, Mathis D, Benoist C. The K/BxN arthritis model. *Curr Protoc Immunol* 2008;Chapter 15:Unit 15.22.
25. Danks L, Komatsu N, Guerrini MM, Sawa S, Armaka M, Kollias G, et al. RANKL expressed on synovial fibroblasts is primarily responsible for bone erosions during joint inflammation. *Ann Rheum Dis* 2016;75:1187–95.
26. Quan L, Zhang Y, Dusad A, Ren K, Purdue PE, Goldring SR, et al. The evaluation of the therapeutic efficacy and side effects of a macromolecular dexamethasone prodrug in the collagen-induced arthritis mouse model. *Pharm Res* 2016;33:186–93.
27. Georgess D, Mazzorana M, Terrado J, Delprat C, Chamot C, Guasch RM, et al. Comparative transcriptomics reveals RhoE as a novel regulator of actin dynamics in bone-resorbing osteoclasts. *Mol Biol Cell* 2014;25:380–96.
28. Leblanc R, Lee SC, David M, Bordet JC, Norman DD, Patil R, et al. Interaction of platelet-derived autotaxin with tumor integrin $\alpha V\beta 3$ controls metastasis of breast cancer cells to bone. *Blood* 2014;124:3141–50.
29. Gupte R, Patil R, Liu J, Wang Y, Lee SC, Fujiwara Y, et al. Benzyl and naphthalene methylphosphonic acid inhibitors of autotaxin with anti-invasive and anti-metastatic activity. *ChemMedChem* 2011;6:922–35.
30. Nakanaga K, Hama K, Aoki J. Autotaxin—an LPA producing enzyme with diverse functions. *J Biochem (Tokyo)* 2010;148:13–24.
31. Fotopoulou S, Oikonomou N, Grigorieva E, Nikitopoulou I, Paparountas T, Thanassopoulou A, et al. ATX expression and LPA signalling are vital for the development of the nervous system. *Dev Biol* 2010;339:451–64.
32. Lee JM, Park H, Noh AL, Kang JH, Chen L, Zheng T, et al. 5-Lipoxygenase mediates RANKL-induced osteoclast formation via the cysteinyl leukotriene receptor 1. *J Immunol* 2012;189:5284–92.
33. Brown AK, Conaghan PG, Karim Z, Quinn MA, Ikeda K, Peterfy CG, et al. An explanation for the apparent dissociation between clinical remission and continued structural deterioration in rheumatoid arthritis *Arthritis Rheum* 2008;58:2958–67.
34. Benesch MG, Tang X, Maeda T, Ohhata A, Zhao YY, Kok BP, et al. Inhibition of autotaxin delays breast tumor growth and lung metastasis in mice *FASEB J* 2014;28:2655–66.
35. Benesch MG, Ko YM, Tang X, Dewald J, Lopez-Campistrous A, Zhao YY, et al. Autotaxin is an inflammatory mediator and therapeutic target in thyroid cancer *Endocr Relat Cancer* 2015;22:593–607.

36. Desroy N, Housseman C, Bock X, Joncour A, Bienvenu N, Cherel L, et al. Discovery of 2-[[2-Ethyl-6-[4-[2-(3-hydroxyazetidin-1-yl)-2-oxoethyl]piperazin-1-yl]-8-methylimidazo[1,2-a]pyridin-3-yl]methylamino]-4-(4-fluorophenyl)thiazole-5-carbonitrile (GLPG1690), a First-in-Class Autotaxin Inhibitor Undergoing Clinical Evaluation for the Treatment of Idiopathic Pulmonary Fibrosis. *J Med Chem* 2017;60:3580–90.
37. Nishioka T, Arima N, Kano K, Hama K, Itai E, Yukiura H, et al. ATX-LPA1 axis contributes to proliferation of chondrocytes by regulating fibronectin assembly leading to proper cartilage formation. *Sci Rep* 2016;6:23433.
38. Panupinthu N, Rogers JT, Zhao L, Solano-Flores LP, Possmayer F, Sims SM, et al. P2X7 receptors on osteoblasts couple to production of lysophosphatidic acid: a signaling axis promoting osteogenesis. *J Cell Biol* 2008;181:859–71.
39. Ferry G, Tellier E, Try A, Grés S, Naime I, Simon MF, et al. Autotaxin is released from adipocytes, catalyzes lysophosphatidic acid synthesis, and activates preadipocyte proliferation. Up-regulated expression with adipocyte differentiation and obesity. *J Biol Chem* 2003;278:18162–69.
40. Kanda H, Newton R, Klein R, Morita Y, Gunn MD, Rosen SD. Autotaxin, an ectoenzyme that produces lysophosphatidic acid, promotes the entry of lymphocytes into secondary lymphoid organs. *Nat Immunol* 2008;9:415–23.
41. Wu J-M, Xu Y, Skill NJ, Sheng H, Zhao Z, Yu M, Saxena R, Maluccio MA. Autotaxin expression and its connection with the TNF-alpha-NF-kappaB axis in human hepatocellular carcinoma. *Mol Cancer* 2010;9:71.

FIGURE LEGENDS

Figure 1: ATX activity blockade has no protective effect on TNF-induced synovitis but reduces TNF-induced bone erosion and systemic bone loss. (A) Photographs of hind paw swelling from *hTNF^{+/-}* mice 14 days after the initiation of vehicle or BMP22 treatment and mice weight, hind paw thickness and arthritis score from *hTNF^{+/-}* mice during treatment period. Empty triangles: vehicle-treated *hTNF^{+/-}* mice, black squares: BMP22-treated *hTNF^{+/-}* mice. Data are expressed as means \pm SEM (n=9 per group). (B) Representative HPS staining of hind paws from vehicle-treated *hTNF^{+/-}* and BMP22-treated *hTNF^{+/-}* mice (top panel). Scale bar, 100 μ m. Arrows indicate synovitis. Histologic scores for inflammation (bottom left panel) and bone erosions (bottom right panel) in midfoot of hind paws from vehicle-treated *hTNF^{+/-}* and BMP22-treated *hTNF^{+/-}* mice. (C) Representative three-dimensional micro-CT reconstruction images (top panel) and corresponding bar charts of BS/TV in calcaneus (bottom panel) from vehicle-treated *hTNF^{+/-}* and BMP22-treated *hTNF^{+/-}* mice. Data are expressed as means \pm SEM (n=6 per group). Scale bar, 100 μ m. (D) Representative three-dimensional micro-CT reconstructions of femoral trabecular bone and corresponding bar charts of BV/TV of the distal femoral metaphysis from vehicle-treated *hTNF^{+/-}* and BMP22-treated *hTNF^{+/-}* mice. Data are expressed as means \pm SEM (n=6 per group). (E) Representative TRAP staining of tibiae and corresponding quantification of TRAP positive surface per bone surface (OC.S/BS in %) from vehicle-treated *hTNF^{+/-}* and BMP22-treated *hTNF^{+/-}* mice. Data are expressed as mean \pm SEM (n=6 per group). Scale bars, 100 μ m. (F) Representative immunohistochemistry for ATX (left panel) and TRAP stain (right panel) of hind paws from *hTNF^{+/-}* mice. Scale bar, 100 μ m. Arrows indicate ATX-positive (left) and TRAP-positive (right) multinucleated cells. *p<0.05, **p< 0.01 assessed by Mann-Whitney test.

Figure 2: ATX is expressed by mature OC and is functionally active in resorbing OC. (A) Quantitative RT-PCR (qRT-PCR) analysis for the expression of *Enpp2* at different time of differentiation of murine BMMC into OC upon stimulation with M-CSF and RANKL. Data are expressed as mean \pm SEM. (Inset A) Cell lysates from murine mature OC were analyzed by immunoblot with antibody against ATX. Actin was used as a loading control. (B) TRAP staining and quantification of OC generated from murine BMMC cultured with M-CSF and RANKL, in serum or in charcoal-stripped serum (Charc-serum) supplemented with indicated compound. Values are the mean \pm SEM. Results are representative of 3 independent experiments. (C) Quantification of resorbed mineralized surface by OC. Values are the mean \pm SEM. Results are representative of 3 independent experiments. *p<0.05, ***p<0,001, assessed by ANOVA.

Figure 3: Inhibition of OC-derived ATX expression does not affect bone mass in basal and non-inflammatory osteoporosis conditions.

(A) Cell lysates and corresponding quantification (ATX / Actin ratio) at different time of differentiation into OC of murine BMMC from *CTRL* and Δ ATX^{Ctsk} mice analyzed by immunoblot with antibody against ATX. Actin was used as a loading control. (B) Quantification of resorbed mineralized surface by OC generated from BMMC of Δ ATX^{Ctsk} mice cultured with M-CSF and RANKL in serum or in Charc-serum supplemented or not (NT for non-treated) with LPC alone or together with rATX. Values are the mean \pm SEM. (C) Representative three-dimensional micro-CT reconstruction images and corresponding bar charts of trabecular bone mass quantification with BV/TV of *CTRL* and Δ ATX^{Ctsk} mice (top panel). Data are expressed as means \pm SEM (n=5 per group). Representative TRAP staining of tibiae and corresponding quantification of TRAP positive surface per bone surface (OC.S/BS in %) from *CTRL* and Δ ATX^{Ctsk} mice (bottom panel). Data are expressed as mean \pm SEM (n=5 per group). (D) Representative three-dimensional micro-CT reconstruction images of *CTRL* and Δ ATX^{Ctsk} mice after OVX or Sham operation and corresponding bar charts of trabecular bone loss quantification with % of sham BV/TV. Data are expressed as means \pm SEM (n=9 per group). ***p<0,001 assessed by ANOVA. Scale bars, 100 μ m.

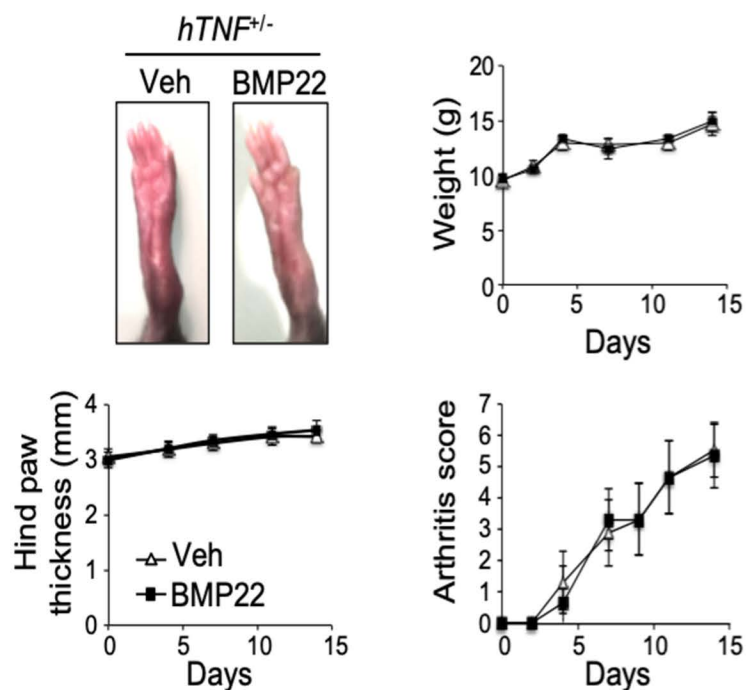
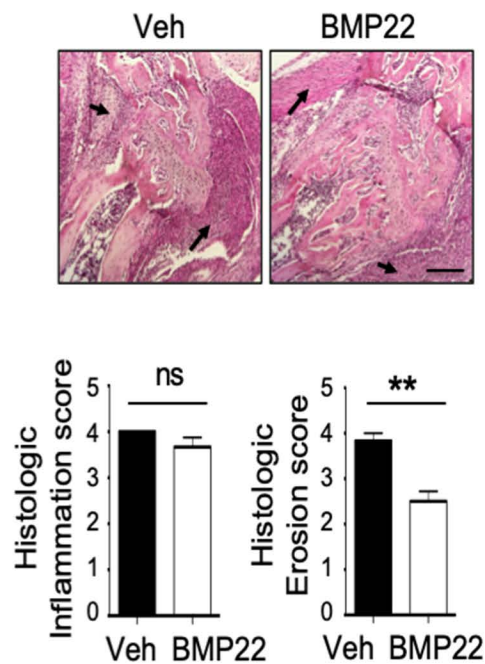
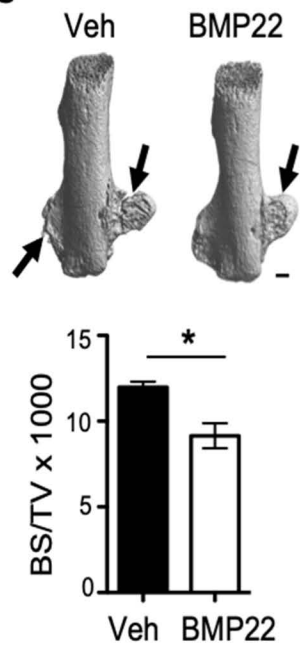
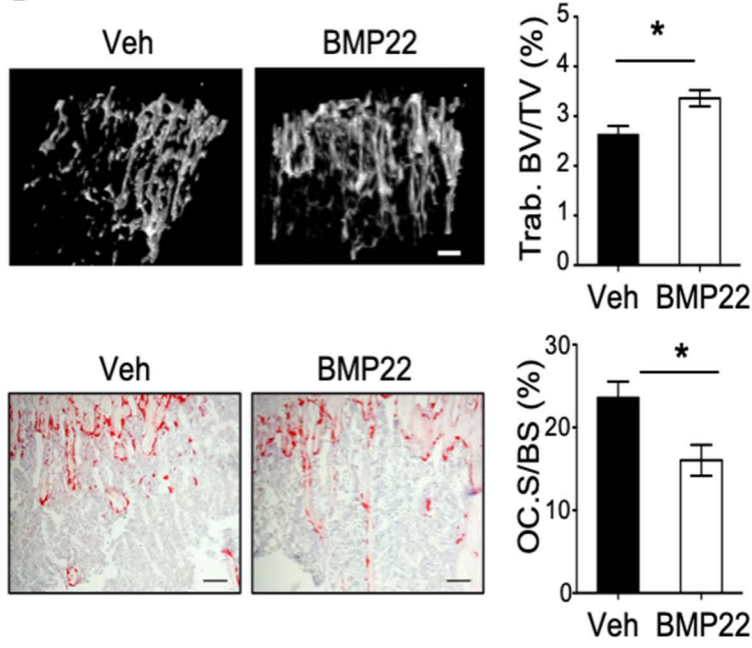
Figure 4: Inhibition of OC-derived ATX expression fully protects mice against LPS-induced bone loss.

(A) Quantification of resorbed mineralized surface by OC generated from *CTRL* and Δ ATX^{Ctsk} murine BMMC cultured with M-CSF and RANKL and seeded for 48h in osteo-assay wells in Charc-serum supplemented with LPC alone or together with TNF (10 ng/ml) or LPS (1 μ g/ml). Values are the mean \pm SEM. (B) Representative three-dimensional micro-CT reconstruction images and corresponding bar charts of femoral trabecular bone mass quantification with BV/TV of *CTRL* and Δ ATX^{Ctsk} mice treated either with LPS or vehicle. Data are expressed as means \pm SEM (n=6 per group). (C) Representative TRAP staining of tibiae and corresponding quantification of TRAP positive surface per bone surface (OC.S/BS in %) from *CTRL* and Δ ATX^{Ctsk} mice treated either with LPS or vehicle. Data are expressed as mean \pm SEM (n=6 per group). (D) qRT-PCR analysis for the expression of *Acp5*, *Ctsk* and *Enpp2*, in long bones from *CTRL* and Δ ATX^{Ctsk} mice treated either with LPS or vehicle (n=6 mice per group). (E) qRT-PCR analysis for the expression of *Enpp2* in *CTRL* mature BMMC-derived OC stimulated for up to 6h by TNF (10 ng/ml) or LPS (1 μ g/ml) and TCPA-1 (2 μ M). Data are expressed as mean \pm SEM. *p<0.05, **p<0.01, ***p<0.001, assessed by ANOVA. Scale bars, 100 μ m.

Figure 5: Mice deficient in OC-derived ATX are partially protected against K/BxN serum transfer-induced bone erosion and systemic bone loss. (A) Representative three-dimensional micro-CT reconstruction images and corresponding bar charts of femoral trabecular bone mass quantification with BV/TV of *CTRL* and Δ *ATX*^{*Ctsk*} mice treated with K/BxN serum or vehicle. Data are expressed as means \pm SEM (n=6 per group). (B) Photographs of hind paw swelling 17 days after the initial serum transfer and hind paw thickness graphs during K/BxN serum transfer period from *CTRL* and Δ *ATX*^{*Ctsk*} mice treated with K/BxN serum or with vehicle. Triangles: *CTRL* mice, squares: Δ *ATX*^{*Ctsk*} mice, empty symbols: vehicle treatment, black symbols: K/BxN serum treatment. Data are expressed as means \pm SEM (n=6 per group). (C) Representative HPS staining (top panel) and TRAP stain (bottom panel) of hind paws from *CTRL* and Δ *ATX*^{*Ctsk*} mice treated with K/BxN. Scale bar, 100 μ m. Stars and arrows indicate respectively synovitis and TRAP-positive multinucleated cells at synovitis-bone interface. (D) Representative three-dimensional micro-CT reconstruction images on hind paws from *CTRL* and Δ *ATX*^{*Ctsk*} mice treated with K/BxN serum or vehicle 17 days after the initial serum transfer. Scale bar, 250 μ m. (E) Representative three-dimensional micro-CT reconstruction images and corresponding bar charts of BS/TV in talus from *CTRL* and Δ *ATX*^{*Ctsk*} mice treated with K/BxN serum or vehicle. Scale bar, 100 μ m. Data are expressed as means \pm SEM (n=6 per group). **p<0.01, ***p<0.001 assessed by ANOVA.

ACKNOWLEDGMENTS

The authors thank Dr Antonios O. Aliprantis for helpful advice. This work was supported by a Passerelle grant from Pfizer (FC) and by grants from INSERM and the University Claude Bernard Lyon-1 (OP), the Comité Départemental de la Loire de la Ligue Contre le Cancer (OP), the French Foundation pour la Recherche sur le Cancer (ARC, Grant n°.PJA20151203151), the ANR grant LYSBONE (OP) (Grant n°. ANR-15-CE14-0010-01), National Cancer Institute CA 092160 (GT). The authors declare no competing financial interests.

A**B****C****D****E**